Convective–radiative heat transfer in a square duct with a centered circular core

Z. F. Dong, M. A. Ebadian, and E. Bigzadeh
Department of Mechanical Engineering, Florida International University, Miami, FL, USA

Combined laminar forced convection and radiation heat transfer have been numerically investigated for a gray, absorbing, emitting, nonscattering gas in the entrance region of a square duct with a centered, circular core. The thermal boundary condition imposed on the square duct and the core is a uniform temperature, both axially and peripherally. The method of moments is applied to consider the radiation contribution. The momentum equation, the three-dimensional energy equation, and the two-dimensional irradiation equation are discretized and numerically solved by the control-volume-based finite-difference method in the boundary-fitted coordinate system. This numerical scheme is found to be simple, accurate, and efficient. The effects of four major parameters influencing combined convective and radiative heat transfer, namely, the geometry parameter, α^*, as well as radiation–conduction, N, optical thickness, τ_b, and wall emissivity, ε_w, are discussed in detail. The results for the total Nusselt number variations indicate that heat transfer is enhanced by thermal radiation. The predicted results for pure convective heat transfer are in good agreement with the available data published in the open literature.

Keywords: combined heat transfer; square duct; numerical technique

Introduction

In energy-related technology, such as coal, oil or gas-fired furnaces, use is made basically of gases heated up to 2000 K. Recently, in missile engineering, the temperature range was widened to 4500 K (Tamonis 1987). Also, nuclear power plants require the application of devices at even higher temperatures. For situations related to nuclear power plants where various processes with high-temperature gaseous working fluids are applied, the combined effects of forced convection and gas radiation must be considered simultaneously. Forced convection in ducts of different cross sections has been extensively studied and published in heat transfer literature. Reviews of this literature carried out by Shah and London (1978) and Kakac *et al.* (1987) and others cited by Eckert *et al.* (1988, 1989, 1991), Soloukhin and Martynenko (1983), and Martynenko (1988) manifest the increasing importance of combined radiative and convective heat transfers, and significant attention has been devoted to this kind of research in the last decade.

Heat treatment of ceramic or metallic products is carried out in different types of ovens. Heat is transferred to the product in the oven by the combined effects of forced convection and gas radiation. Roughly speaking, the oven geometry can be considered as a square duct, where the product inside of it is a centered circular core. This geometric combination has also been considered by several researchers. In the late 1960s, Ratkowsky and Epstein (1968) solved the problem of laminar flow in ducts with centered circular cores without radiation. They employed the method of least-squares fitting of harmonic functions to known boundary conditions to determine the friction factor. Point matching methods have been applied to fully developed laminar flow by Cheng and Jamil (1967) to calculate heat transfer in noncircular annular ducts having a central circular core governed by the thermal boundary conditions of uniform heat flux from each wall and equal wall temperatures. However, the Cheng and Jamil (1967) investigation did not take into consideration the effects of radiation. Yang *et al.* (1989) and Yang and Ebadian (1992) considered the effects of combined radiation and forced convection in ducts of different cross sections. Im and Ahluwalia (1984) analyzed combined convective and radiative heat transfer by solving simultaneously the fluid dynamic equations and the radiation transport equation. However, the solution of these problems has been restricted to conditions involving simple ducts without a centered circular core.

Therefore, the objective of this paper is to present a numerical solution of combined convection and radiation heat transfer in laminar flow in a square duct with a centered circular core. In general, accounting for convective–radiative laminar flow with developing temperature in a square duct with a centered circular core is a difficult problem. One of the difficulties is dealing with the combined convection and radiation problem. The energy and radiation transport equations are coupled together and must be solved simultaneously in order to determine the local temperature and heat transfer rates. In the case of radiation, the energy balance is expressed in terms of a nonlinear, integrodifferential equation. Solution of this problem requires considerable computational time to perform spectral calculations. Fortunately, to avoid these difficulties, the radiation problem has been modeled by the method of moments, wherein the radiative transfer equation is expressed in differential form (cf. Özisik 1973). The advantage of this differential approach is that the radiative transport equation (RTE) becomes a partial differential equation of an elliptic type. Consequently, the RTE is adapted to a general, diffusion–convection type of equation to perform the numerical analysis. On the other hand, due to the geometric complexity of the square duct with a centered

Address reprint requests to Professor Ebadian at the Department of Mechanical Engineering, Florida International University, Miami, FL 33199, USA.

Received 13 January 1992; accepted 9 June 1992

circular core, the numerically generated boundary-fitted coordinate system is applied to discretize the solution domain. Accordingly, the governing equations for combined radiation–convection are formulated in the boundary-fitted coordinate system and then solved successively. Therefore, the numerical results are presented in terms of the distribution of the total Nusselt number for four major parameters: namely, the geometry parameters, optical thickness, the radiation–conduction parameter, and wall emissivity.

Problem formulation

The geometry under consideration is shown in Figure 1 and is designated as a straight duct of square cross section with a centered circular pipe. The flow in the duct is considered to be hydrodynamically fully developed laminar flow. In this paper, the emphasis is on the entrance region of the duct where combined convective–radiative heat transfer occurs. At $Z = 0$, the gas temperature is equal to T_e, and for $Z > 0$, the surface of the duct and the outer surface of the pipe are uniform and equal, $T_w = T_p$. As mentioned above, radiation will be modeled by the method of moments, with the assumption that the participating gas is gray, emitting, absorbing, and nonscattering. Strictly speaking, radiation and convection in the entrance region are three-dimensional (3-D). However, axial conduction and axial radiation can be neglected under certain conditions. For example, Shah and London (1978) pointed out that axial conduction for pure forced convection is negligible when the Peclet number is greater than 50 in the case of a constant wall temperature, and greater than 10 in the case of constant heat flux. Sparrow and Cess (1978) provided the criteria of

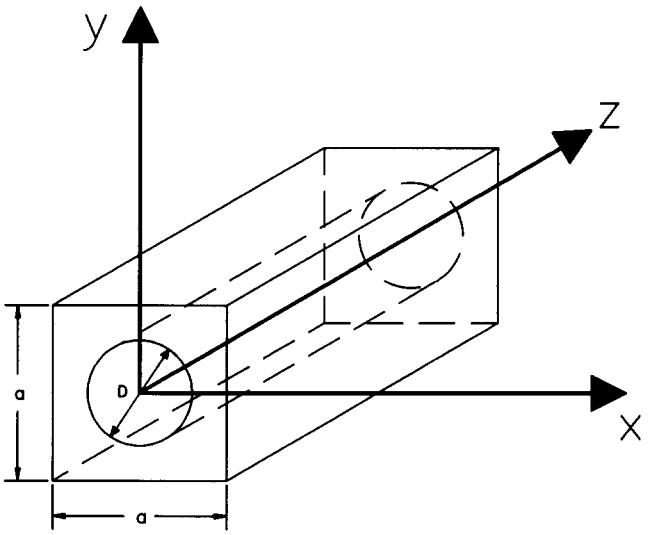

Figure 1 Geometry

Notation

A	Cross-section area [m^2]
a	Length of the square duct [m]
c_p	Specific heat capacity at constant pressure [$J\,kg^{-1}\,K^{-1}$]
D	Pipe diameter [m]
D_h	Hydraulic diameter
F	Dependent variable
f	Friction factor
G^*	Total irradiation [$W\,m^{-2}$]
G	Dimensional value of $G' = G/4\sigma T_w^4$
h	Heat transfer coefficient [$W\,m^{-2}\,K^{-1}$]
J	Jacobian transformation
k	Thermal conductivity [$W\,m^{-1}\,K^{-1}$]
N	Radiation conduction parameter, $4\sigma T_w^3/k\kappa$
Nu	Nusselt number, hD_h/k
n	Outward normal direction on boundary
P	Perimeter [m], pressure [Pa]
Pe	Peclet number, Re Pr
Pr	Prandtl number, ν/α_T
q	Heat flux [$W\,m^{-2}$]
Re	Reynolds number, $W_m D_h/\nu$
T	Temperature of fluid [K]
W	Dimensional velocity [ms^{-1}]
W_m	Dimensional mean velocity [ms^{-1}], $1/A \iint W dA$
w	Dimensionless velocity, $-\mu/a^2\, W/dP/dZ$
w_m	Dimensionless mean velocity, $1/A \iint w dA$
X, Y	Dimensional transversal coordinates
x, y	Dimensionless transversal coordinates, X/a, Y/a
Z	Dimensional axial coordinate
z	Dimensionless axial coordinate, Z/D_hPe

Greek symbols

α	Coefficient, Equation 23
α^*	Geometry parameter, D/a
α_T	Thermal diffusivity [$m^2\,s^{-1}$]
β	Coefficient, Equation 24, extinction coefficient [m^{-1}]
γ	Coefficient, Equation 25
ε_w	Emissivity of wall
θ	Dimensionless temperature, $\frac{T}{T_w}$
θ_b	Dimensionless bulk temperature, $\frac{T_b}{T_w}$
θ_e	Dimensionless inlet temperature, $\frac{T_e}{T_w}$
κ	Volumetric absorption coefficient [m^{-1}]
λ	Coefficient, Equation 16
μ	Dynamic viscosity [$kg\,m^{-1}\,s^{-1}$]
ν	Kinematic viscosity [$m^2\,s^{-1}$]
ρ	Density [$kg\,m^{-3}$]
σ	Stefan–Boltzmann constant [$W\,m^{-2}\,K^{-4}$]
τ_b	Optical thickness, κD_h
ϕ	Coefficient, Equation 27
ψ	Coefficient, Equation 26
ξ, η	Transversal coordinates in the computational plane

Subscripts

b	Bulk
c	Convection
e	Entrance
m	Mean
max	Maximum
p	Pipe
r	Radiation
T	Total
w	Wall (circumferential)
∞	Asymptotic value

$\mathrm{Pe}\,\tau_b/N \gg 10$ for axial radiation to be negligible. Also, the investigation by Yang and Ebadian (1991) indicated that the effects of radiation in the axial direction are negligible when $\mathrm{Pe}\,\tau_b/N > 10$. Therefore, based on the above-cited references, heat conduction and radiation in the axial direction are disregarded in this paper. Furthermore, the thermal properties of Newtonian fluid are assumed to be constant. Thus, the corresponding governing equations are as follows.

Momentum equation

$$\frac{\partial^2 W}{\partial X^2} + \frac{\partial^2 W}{\partial Y^2} = \frac{1}{\mu}\frac{dP}{dZ} \tag{1}$$

In dimensionless form,

$$\frac{\partial^2 w}{\partial x^2} + \frac{\partial^2 w}{\partial y^2} + 1 = 0 \tag{2}$$

where

$$w = \frac{\mu W}{-\frac{dP}{dZ}a^2}, \qquad x = \frac{X}{a}, \qquad y = \frac{Y}{a}$$

Due to the symmetry, only a quarter of the cross section of the duct is considered for the computational domain. The boundary conditions applied to the momentum equation, Equation 2, are as follows:

$$w = 0 \qquad \text{on the walls of the duct and on the pipe} \tag{3}$$

$$\frac{\partial w}{\partial n} = 0 \qquad \text{on the symmetrical line} \tag{4}$$

Energy and irradiation equations

The energy equation may be expressed as

$$\rho c_p W \frac{\partial T}{\partial Z} = k\left[\frac{\partial^2 T}{\partial X^2} + \frac{\partial^2 T}{\partial Y^2}\right] + \kappa(G^* - 4\sigma T^4) \tag{5}$$

where irradiation, G^*, is determined from integration of the RTE. Due to the large Peclet number, the axial radiation effect is neglected, and by using the method of moments, irradiation, G^*, is expressed by the following equation:

$$\frac{\partial^2 G^*}{\partial X^2} + \frac{\partial^2 G^*}{\partial Y^2} = 3\beta\kappa(G^* - 4\sigma T^4) \tag{6}$$

where β in Equation 6 represents the extinction coefficient. For nonscattering gas,

$$\beta = \kappa \tag{7}$$

Upon introduction of the following dimensionless variables and parameters,

$$\bar{w} = \frac{W}{W_m}, \qquad \theta = \frac{T}{T_w}, \qquad x = \frac{X}{a}, \qquad y = \frac{Y}{a}$$

$$z = \frac{Z}{D_h \mathrm{Pe}}, \qquad \mathrm{Re} = \frac{W_m D_h}{\nu}, \qquad \mathrm{Pe} = \mathrm{Re}\,\mathrm{Pr}$$

$$D_h = \frac{a\left(1 - \alpha^{*2}\frac{\pi}{4}\right)}{\left(1 + \alpha^*\frac{\pi}{4}\right)}, \qquad \alpha^* = \frac{D}{a} \tag{8}$$

$$N = \frac{4\sigma T_w^3}{k\kappa}, \qquad \tau_b = \kappa D_h, \qquad G = \frac{G^*}{4\sigma T_w^4}$$

the energy equation (Equation 5) and irradiation equation (Equation 6) can be written in dimensionless form as

$$\left(\frac{a}{D_h}\right)^2 \bar{w}\frac{\partial \theta}{\partial z} = \frac{\partial^2 \theta}{\partial x^2} + \frac{\partial^2 \theta}{\partial y^2} + N\tau_b^2\left(\frac{a}{D_h}\right)^2 (G - \theta^4) \tag{9}$$

$$\frac{\partial^2 G}{\partial x^2} + \frac{\partial^2 G}{\partial y^2} = 3\tau_b^2\left(\frac{a}{D_h}\right)^2 (G - \theta^4) \tag{10}$$

The boundary conditions for Equation 9 are

$$\theta_p = 1, \quad \theta_w = 1 \qquad \text{on the wall of the duct and on the pipe} \tag{11}$$

$$\frac{\partial \theta}{\partial n} = 0 \qquad \text{on the symmetry line} \tag{12}$$

$$\theta = \theta_e \qquad \text{on the entrance } z = 0 \tag{13}$$

Also the irradiation equation, Equation 10, is subjected to boundary conditions on the wall of the duct and on the pipe

$$\frac{\partial G}{\partial n} = -\frac{3}{2}\lambda_w \tau_b\left[\frac{a}{D_h}\right](G_w - 1) \tag{14}$$

and on the symmetry line,

$$\frac{\partial G}{\partial n} = 0 \tag{15}$$

where in Equation 14

$$\lambda_w = \frac{\varepsilon_w}{2 - \varepsilon_w} \tag{16}$$

and ε_w is the wall emissivity.

Parameters of interest

The hydrodynamic characteristics of the duct flow may be conveniently represented by the product of the friction factor, f, and the Reynolds number, Re. The conventional definition would be

$$f\mathrm{Re} = \frac{2}{w_m}\left(\frac{D_h}{a}\right)^2 \tag{17}$$

The thermal characteristics of the fluid inside any duct is represented by a dimensionless bulk temperature, defined as

$$\theta_b = \frac{\int_A w\theta dA}{\int_A w dA} \tag{18}$$

where

$$\theta = \frac{T}{T_w} \tag{19}$$

By considering the energy conservation equation, the Nusselt number is found to be

$$\mathrm{Nu}_T = -\frac{1}{4}\frac{1}{(1 - \theta_b)}\frac{d\theta_b}{dz} \tag{20}$$

Equation 20 can be obtained based on the assumption that the duct and the pipe walls have the same temperature.

Solution procedure

Numerical grid generation

A numerically generated boundary-fitted coordinate system is applied to resolve the difficulty of discretization due to the complex boundaries. The boundary-fitted coordinate technique has been explained in detail by Thompson *et al.* (1985). According to this publication, the domain transformation between the physical coordinates (x, y) and the transversal coordinates (ξ, η) in the computational plane is achieved by solving the two coupled equations

$$\alpha\left(\frac{\partial^2 x}{\partial \xi^2}+\phi\frac{\partial x}{\partial \xi}\right)-2\beta\frac{\partial^2 x}{\partial \xi\,\partial \eta}+\gamma\left(\frac{\partial^2 x}{\partial \eta^2}+\psi\frac{\partial x}{\partial \eta}\right)=0 \tag{21}$$

$$\alpha\left(\frac{\partial^2 y}{\partial \xi^2}+\phi\frac{\partial y}{\partial \xi}\right)-2\beta\frac{\partial^2 y}{\partial \xi\,\partial \eta}+\gamma\left(\frac{\partial^2 y}{\partial \eta^2}+\psi\frac{\partial y}{\partial \eta}\right)=0 \tag{22}$$

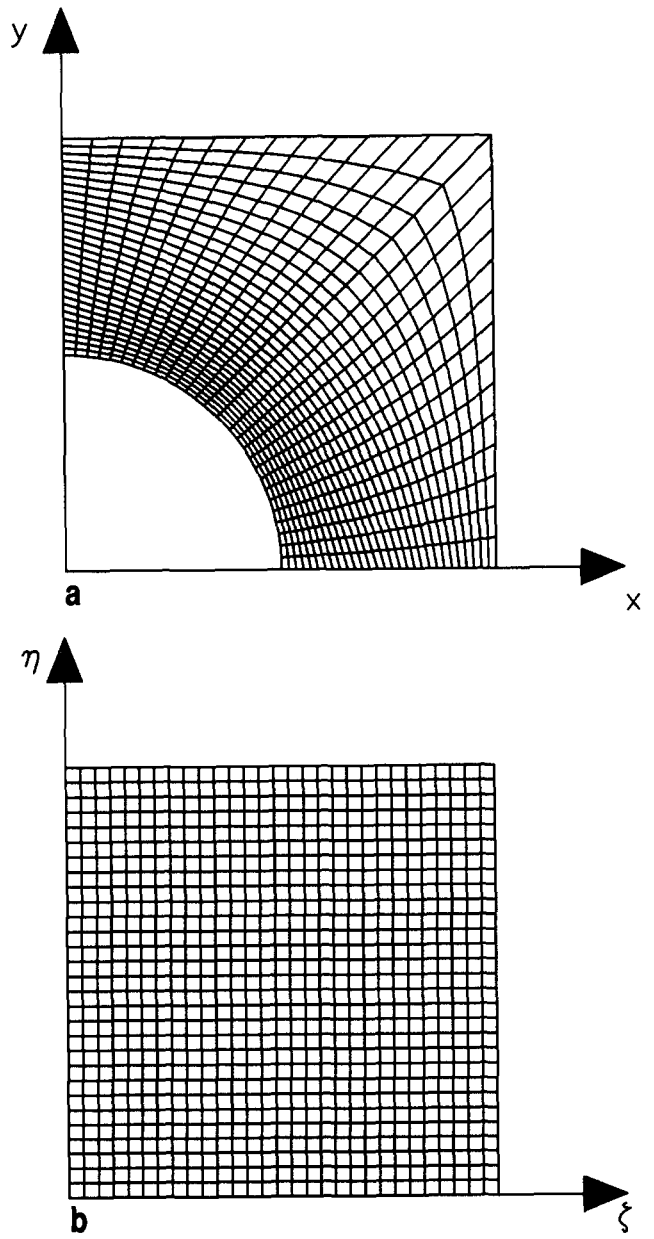

Figure 2 Grid configuration. (a) Physical plane, (b) computational plane

where

$$\alpha=\left(\frac{\partial x}{\partial \eta}\right)^2+\left(\frac{\partial y}{\partial \eta}\right)^2 \tag{23}$$

$$\beta=\frac{\partial x}{\partial \xi}\frac{\partial x}{\partial \eta}+\frac{\partial y}{\partial \xi}\frac{\partial y}{\partial \eta} \tag{24}$$

$$\gamma=\left(\frac{\partial x}{\partial \xi}\right)^2+\left(\frac{\partial y}{\partial \xi}\right)^2 \tag{25}$$

On the left and right boundaries of the domain in the computational plane,

$$\psi=-\frac{\left(\dfrac{\partial^2 y}{\partial \eta^2}\dfrac{\partial y}{\partial \eta}+\dfrac{\partial^2 x}{\partial \eta^2}\dfrac{\partial x}{\partial \eta}\right)}{\left[\left(\dfrac{\partial x}{\partial \eta}\right)^2+\left(\dfrac{\partial y}{\partial \eta}\right)^2\right]} \tag{26}$$

On the top and bottom boundaries of the domain in the computational plane,

$$\phi=-\frac{\left(\dfrac{\partial^2 x}{\partial \xi^2}\dfrac{\partial x}{\partial \xi}+\dfrac{\partial^2 y}{\partial \xi^2}\dfrac{\partial y}{\partial \xi}\right)}{\left[\left(\dfrac{\partial x}{\partial \xi}\right)^2+\left(\dfrac{\partial y}{\partial \xi}\right)^2\right]} \tag{27}$$

The ϕ and ψ values on the internal grid points are determined by linear interpolation from the boundary values. The resulting grid construction in the physical plane and in the computational plane is shown in Figures 2a and 2b.

Governing equations in the computational plane

It is necessary to transfer the governing equations, Equations 9 and 10, in the physical plane to those in the computational plane as follows:

$$\frac{\partial^2 w}{\partial \xi^2}+\frac{\partial^2 w}{\partial \eta^2}+J=0 \tag{28}$$

$$J\bar{w}\left(\frac{a}{D_h}\right)^2\frac{\partial \theta}{\partial z}=\frac{\partial}{\partial \xi}\left[\frac{1}{J}\left(\alpha\frac{\partial \theta}{\partial \xi}-\beta\frac{\partial \theta}{\partial \eta}\right)\right]+\frac{\partial}{\partial \eta}\left[\frac{1}{J}\left(\gamma\frac{\partial \theta}{\partial \eta}-\beta\frac{\partial \theta}{\partial \xi}\right)\right]+JN\tau_b^2\left(\frac{a}{D_h}\right)^2(G-\theta^4) \tag{29}$$

$$\frac{\partial}{\partial \xi}\left[\frac{1}{J}\left(\alpha\frac{\partial G}{\partial \xi}-\beta\frac{\partial G}{\partial \eta}\right)\right]+\frac{\partial}{\partial \eta}\left[\frac{1}{J}\left(\gamma\frac{\partial G}{\partial \eta}-\beta\frac{\partial G}{\partial \xi}\right)\right]-3J\tau_b^2\left(\frac{a}{D_h}\right)^2(G-\theta^4)=0 \tag{30}$$

where

$$J=\frac{\partial x}{\partial \xi}\frac{\partial y}{\partial \eta}-\frac{\partial x}{\partial \eta}\frac{\partial y}{\partial \xi} \tag{31}$$

Since the velocity field for laminar flow is independent of the temperature field, Equation 28 can be solved first; therefore, the velocity distribution will be used in the process of solving the energy and the irradiation equations. However, inspection of Equations 29 and 30 indicates that these two equations are coupled together and must be solved simultaneously. Using the control-volume-based finite-difference approach (Patankar 1980), the energy equation, Equation 29, and the irradiation equation, Equation 30, are discretized to form two sets of algebraic equations, where the statement $\dfrac{\partial^2}{\partial \xi\,\partial \eta}$ is treated as an

Table 1 Independent grid test

$\alpha^* = \frac{D}{\alpha}$	Grid number	f Re
0.8	40 × 40	75.76
	30 × 30	75.40
	20 × 20	73.92
0.5	40 × 40	90.05
	30 × 30	89.28
	20 × 20	87.53
0.2	30 × 30	91.01
	20 × 20	89.68

additional source term. Because of the parabolic characteristics of the energy equation, the computation is marched from the entrance to the exit of the duct. In each marching step, the nonlinearity of the source term and the coupled characteristics of Equations 29 and 30 require the use of iteration for obtaining the convergent solution. The following convergence criterion is chosen in this study:

$$\frac{\|F_{ij}^{k+1} - F_{ij}^{k}\|_{\infty}}{\|F_{ij}^{k}\|} \leqslant 10^{-4}$$

where F refers to the dependent variables, θ and G, respectively; k stands for the kth iteration; and $\|\cdot\|_{\infty}$ is the infinite norm. When the convergent temperature field is reached, the local bulk temperature and the Nusselt number can be calculated from Equations 18 and 20 for the axial location.

As seen in Table 1, a numerical independent grid test has been performed to determine the number of grids and marching step size in the axial direction. Comparison of the fRe values in this table indicates less than 1 percent difference between the finer grid of 40 × 40 and the coarser grid of 30 × 30. Therefore, the 30 × 30 grid has been used in this computation. As described by Tamonis (1987), Yang *et al.* (1989), and Yang and Ebadian (1992), the Nusselt number for combined convective and radiative heat transfer usually increases near the exit where radiation dominates convection. For the purpose of carefully examining the Nusselt-number variations in the axial direction, the uniform axial marching step size, $\Delta z = 1.25 \times 10^{-4}$, is applied.

The validity of the present solution is confirmed by calculating the thermal developing flow for pure convection in the entrance region of the square duct, which is the special case of the present study ($\alpha^* = 0$). The results have been compared with data from Kakac *et al.* (1987), and excellent agreement is noted. The maximum discrepancy between these results is less than 0.6 percent. Also, the product of the fRe for fully developed flow in a square duct from the present computation (fRe = 14.227) is compared with the fRe from Shah and London (1978) (fRe = 14.201), which also indicates excellent agreement.

Results and discussion

A numerical investigation has been performed on combined convective and radiative heat transfer for laminar flow in a square duct with a centered circular core, which has a uniform temperature equal to that of the square duct. In this investigation, attention is focused on the thermal entrance region. Numerical solutions are obtained for a variety of combinations of the following parameters: optical thickness, τ_b; radiation–conduction parameter, N; wall emissivity, ε_w; and the geometry parameter, α^*. The effect of each parameter on the flow and heat transfer is discussed in the following section.

First, the discussion deals with laminar forced convection in a square duct with a centered circular core (Figure 3). The product of the friction factor and the Reynolds number, fRe, and the Nusselt number, Nu_{∞}, for fully developed laminar flow are displayed in this figure for the purpose of showing the influence of the geometry parameter, $\alpha^* = D/a$. In addition, the data provided by Shah and London (1978) for the fRe are also indicated in this figure in the form of a full circle. It is observed that the values of fRe between the present computations and those of Shah and London (1978) are very close. Furthermore, these data also verify the accuracy of the present calculations. Inspection of this figure reveals that the Nusselt number variations have a tendency differing from the fRe. Furthermore, it is seen that the Nusselt number initially increases as α^* increases, and subsequently decreases after $\alpha^* > 0.5$. Finally, it is observed that both fRe and Nu_{∞} are greater for the duct under consideration than those for a square duct. One can explain this by the fact that the centered circular core provides more surface contacting the fluid, which results in enhancement of both the fRe and the Nu.

Figures 4a, 4b, and 4c show the velocity contour for the fully developed flow in a square duct with a centered circular core for $\alpha^* = 0.2$, 0.5, and 0.8, respectively. The common factor of these figures are that four-eyes appear in the cross-section duct. The center "eyes" are located in the diagonals of the square. When the geometry parameters increase, the "eyes" become larger. This is attributed to the fact that the cross section of the duct decreases as the geometry parameter increases. It seems that the velocity distribution is unchanged qualitatively as the geometry parameters vary.

Figure 5 depicts the axial variation of the total Nusselt number for pure convection with α^* as a parameter. As expected, the Nusselt number decreases from a large value at the inlet of the duct to an asymptotic value downstream. Figure 5 illustrates that the effect of the parameter, α^*, on heat transfer for pure forced convection is insignificant.

Figure 6 represents the total Nusselt number variation along the axial direction in the case of wall emissivity, $\varepsilon_w = 1.0$, the radiation–conduction parameter, $N = 5$, and optical thickness, $\tau_b = 5$ as the geometry parameter, α^*, varies from 0.2 to 0.8. It is seen from this figure that the $Nu_{Z,T}$ has a higher value initially and gradually decreases to a minimum value at a certain downstream location and increases again in spite of the value for the geometry parameter, α^*. It is also found from Figure 6 that the total Nusselt number in the entrance region increases

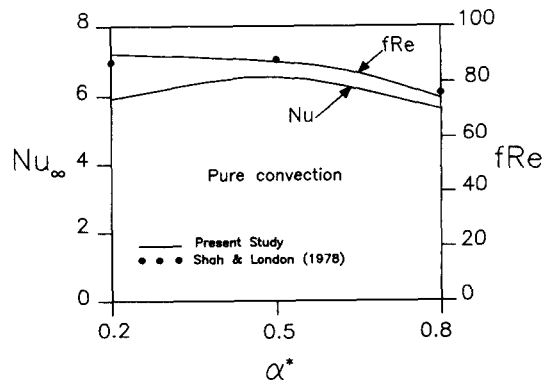

Figure 3 fRe and Nu_{∞} for the fully developed laminar flow

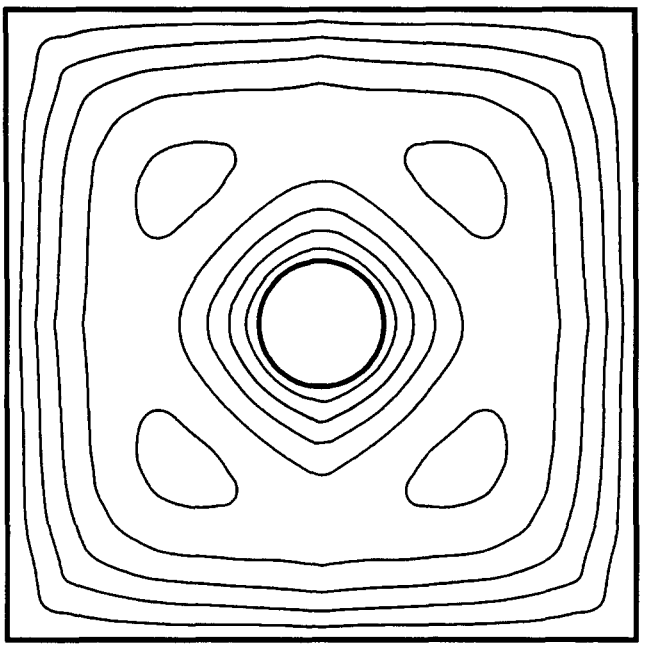

Figure 4 Axial velocity contour. (a) $\alpha^* = 0.2$, $\frac{W_{max}}{W_m} = 1.67$; (b) $\alpha^* = 0.5$, $\frac{W_{max}}{W_m} = 1.84$; (c) $\alpha^* = 0.8$, $\frac{W_{max}}{W_m} = 2.53$

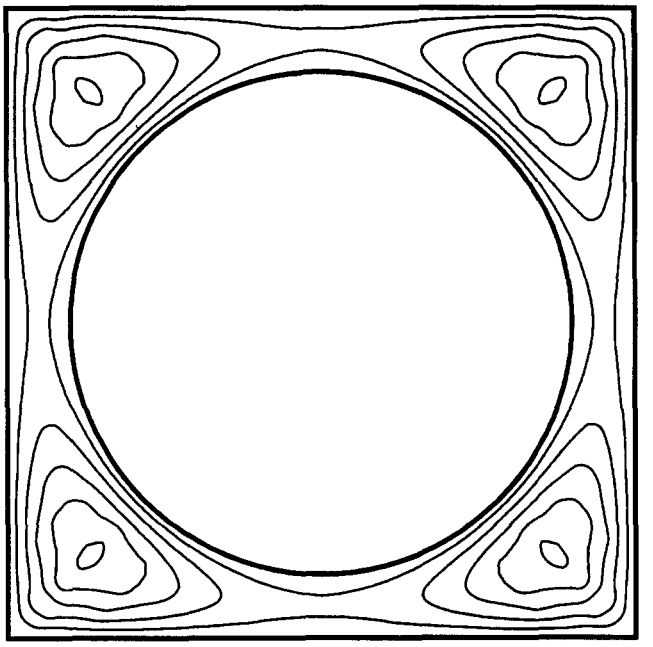

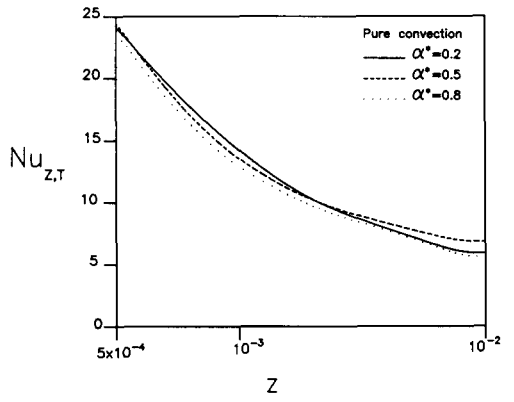

Figure 5 Nusselt number variation for pure convection

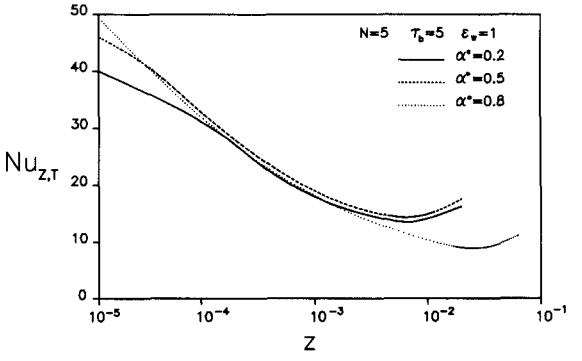

Figure 6 Effects of geometry parameter on the total Nusselt number

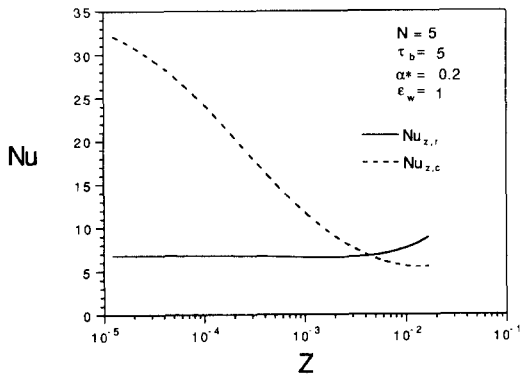

Figure 7 Axial variation of $Nu_{z,c}$ and $Nu_{z,r}$ when $\alpha^* = 0.2$

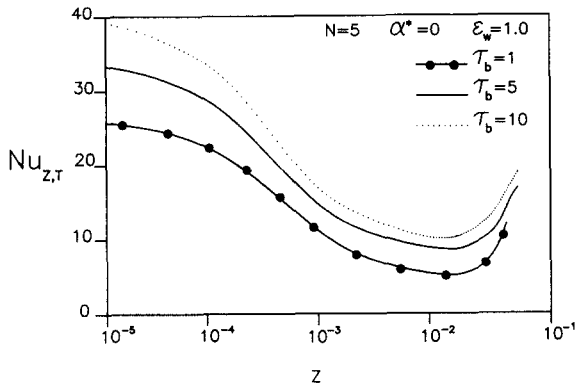

Figure 8 Effects of optical thickness on the total Nusselt number

as the geometry parameter, α^*, increases; whereas downstream, the Nusselt number for $\alpha^* = 0.2$ is larger than that for $\alpha^* = 0.5$, and is lower than that for $\alpha^* = 0.8$. For combined convective and radiative heat transfer, $Nu_{z,T}$ is composed of two parts, $Nu_{z,c}$, which is the Nusselt number for convection, and $Nu_{z,r}$, which is the Nusselt number for radiation. Variations of each are shown in Figure 7 for $\alpha^* = 0.2$. The other fixed parameters are the same as in Figure 6. $Nu_{z,c}$ decreases monotonously from a larger value at the entrance to a small value downstream. However, $Nu_{z,r}$ increases from a small value at the entrance to a larger value downstream. Physically, at the entrance, the thermal boundary layer thickness is very small. Therefore, convective heat transfer is dominant, with radiation having only a moderate effect. As the thermal boundary thickness increases in the flow direction, convective heat transfer is reduced and radiative heat transfer intensifies. However, the increase in the radiative Nusselt number, $Nu_{z,r}$, is smaller than the decrease in the convective Nusselt number, $Nu_{z,c}$, which results in the total Nusselt number, $Nu_{z,T}$, decreasing. After a certain axial location, the Nusselt number for convection approaches an asymptotic value, where the entire duct is the thermal boundary while radiation heat transfer is still increasing. This is because the total Nusselt number, $Nu_{z,T}$, increases in a downstream location of the duct (Figure 6).

Figure 8 shows the effects of optical thickness, τ_b, on the Nusselt number with $N = 5$ and $\varepsilon_w = 1.0$ and with the limiting case of $\alpha^* = 0$, which represents a rectangular duct. It is seen that at any axial location, the Nusselt number increases as the optical thickness, τ_b, increases. The Nusselt number decreases from a large value at the entrance region to a minimum value at almost the same downstream location for all three different values of τ_b, and then increases again.

Figure 9 displays the effects of radiation-conduction parameter, N, on combined convective and radiative heat transfer. This figure is drawn for conditions of $\tau_b = 2$, $\alpha^* = 0.5$, and $\varepsilon_w = 1$. The radiation-conduction parameter, N, varies from 1 to 5. It is obvious that the radiation-conduction parameter has a positive effect on the local Nusselt number; that is, the Nusselt number increases as N increases. A similar tendency of the Nusselt number variation is observed where $N = 1$, 3, and 5.

The effects of wall emissivity, ε_w, on the total Nusselt number are shown in Figure 10. The parameters corresponding to this figure are $N = 5$, $\tau_b = 5$, and $\alpha^* = 0.5$. Three curves for $\varepsilon_w = 0.1$, 0.5, and 1.0 are plotted. It is apparent that the larger the wall emissivity, the greater the local Nusselt number. This means that a high wall emissivity would lead to a high Nusselt number on the wall. Like the effects of N and τ_b on the Nusselt number, the total Nusselt number has a similar tendency in the axial direction. In addition, comparison of the Nusselt number in Figures 8 and 10 indicates that the presence of the circular core can increase the values of the total Nusselt number. Therefore, based on the foregoing results, one can conclude that the heat transfer behavior of combined radiation and forced convection is quite different from that of pure convection. It is observed that in the region close to the inlet of the square duct, forced convection is dominant, and therefore, the effects of radiation are weak and the total Nusselt number decreases monotonously. At a certain location, the total Nusselt number reaches a minimum value as the flow develops, and after that, radiation is stronger and dominant; thus, the total Nusselt number finally increases. It is concluded that the thermally fully

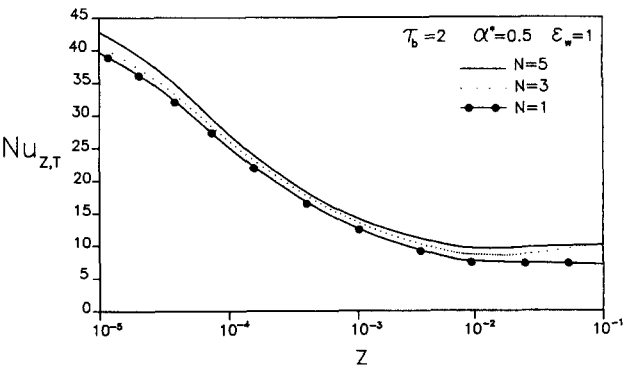

Figure 9 Effects of radiation-conduction on the total Nusselt number

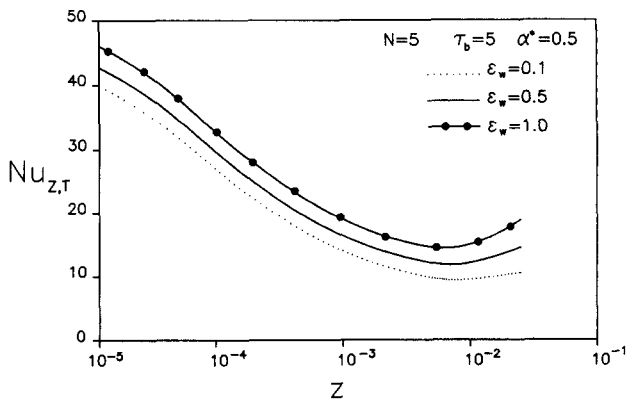

Figure 10 Effects of wall emissivity on the total Nusselt number

developed state is never reached in the case of combined radiation and convection. This verifies the results reported by other researchers (Yang *et al.* 1989; Yang and Ebadian 1992; Smith and Shen 1983; Schmidt *et al.* 1982). Furthermore, the higher values of τ_b, N, and ε_w will enhance heat transfer in the duct.

Concluding remarks

In this paper, combined convective and radiative heat transfer have been examined for thermal developing laminar flow in a square duct with a centered circular core. The significant role played by radiation in the thermal entrance region has been analyzed by the method of moments. The momentum, energy, and irradiation equations have been discretized by the use of the boundary-fitted coordinate system and solved successively. The effects of the radiation–conduction parameter, N, optical thickness, τ_b, geometry parameter, α^*, and wall emissivity, ε_w, on heat transfer in the entrance region of the square duct with a centered circular core have been investigated. It has been observed that the total Nusselt number decreases from a large value at the inlet of the square duct to a minimum value at a certain downstream location, and then increases. This indicates that at the entrance region, convective heat transfer is dominant, whereas radiation becomes dominant downstream. The total Nusselt number at any axial location for combined convection and radiation heat transfer is greater than that for pure convection alone. The major parameters affecting radiation heat transfer are the radiation–conduction parameter, N, optical thickness, τ_b, and wall emissivity, ε_w. Increasing the value for any of these parameters will result in the enhancement of heat transfer. The geometry parameter, α^*, has only a significant effect on combined convective–radiative heat transfer. In addition, the Nusselt number for the square duct with a centered circular core is higher than that for the square duct without a core in the case of combined convective–radiative heat transfer, as well as for pure convection.

In many engineering applications, a detailed analysis may be required to study radiation heat transfer with a participating medium of nongray gas having absorbing, emitting, and scattering properties, as well as the spectral effect and wall reflection, where the method of moments fail, to model radiation. Therefore, this work could be extended to encompass the nongray behavior of gases and the nature of scattering, although a good approximation for radiation is achieved by the method of moments for complex geometry, such as a square duct with a centered circular core.

Acknowledgment

The results presented in this paper were obtained in part in the course of research sponsored by the National Science Foundation under Grant No. CTS-9017732.

References

Cheng, K. C. and Jamil, M. 1967. Laminar flow and heat transfer in ducts of multiple cross sections. *ASME-AIChE*, **67-HT-6**, 1–9

Eckert, E. R. G., Goldstein, R. G., Ibele, W. E., Patankar, S. V., Simon, T. W., Decker, N. A., Girshick, S. L., Strykowski, P. J., Tamma, K. K., Bar-Cohen, A., Herbelein, J. V. R. and Hofeldt, D. L. 1991. Heat transfer—a review of the 1990 literature. *Int. J. Heat Mass Transfer*, **34** (12), 2931–3010

Eckert, E. R. G., Goldstein, R. G., Pfender, E., Ibele, W. E., Patankar, S. V., Simon, T. W., Decker, N. A., Lee, H. O., Girshick, S. L., Scott, C. J., Strykowski, P. J. and Tamma, K. K. 1989. Heat transfer—a review of the 1988 literature. *Int. J. Heat Mass Transfer*, **32**, 2211–2280

Eckert, E. R. G., Goldstein, R. G., Pfender, E., Ibele, W. E., Patankar, S. V., Ramsey, S. W., Simon, T. W., Decker, N. A., Kuehn, T. H., Lee, H. O. and Girshick, S. L. 1988. Heat transfer—a review of the 1987 literature. *Int. J. Heat Mass Transfer*, **31**, 2404–2488

Im, K. H. and Ahluwalia, R. K. 1984. Combined convection and radiation in rectangular ducts. *Int. J. Heat Mass Transfer*, **27** (2), 221–231

Kakac, S., Shah, R. K. and Aung, W. 1987. *Handbook of Single-Phase Convection Heat Transfer*. Wiley Interscience, New York

Martynenko, O. G. 1988. Heat and mass transfer bibliography—Soviet literature. *Int. J. Heat Mass Transfer*, **31**, 2489–2503

Özisik, N. 1973. *Radiative Heat Transfer*. John Wiley, New York.

Patankar, S. V. 1980. *Numerical Heat Transfer and Fluid Flow*. Hemisphere, Washington, DC

Ratkowsky, D. A. and Epstein, N. 1968. Laminar flow in regular polygonal shaped ducts with circular centered cores. *Can. J. Chem. Eng.*, **46**, 22–26

Schmidt, C. A., Yener, Y. and Özisik, M. N. 1982. Simultaneous convection and radiation in participating laminar flow between parallel plates. *16th Southeastern Semin. Thermal. Sci.*, Miami Beach, FL

Shah, R. K. and London, A. L. 1978. *Laminar Flow Forced Convection in Ducts*. Academic Press, New York

Smith, T. F. and Shen, Z. F. 1983. Radiative transfer and convective transfer in a cylindrical enclosure. *ASME*, **83-HT-53**

Soloukhin, R. I. and Martynenko, O. G. 1983. Heat and mass transfer bibliography—Soviet literature. *Int. J. Heat Mass Transfer*, **26**, 1771–1781

Sparrow, E. M. and Cess, R. D. 1978. *Radiation Heat Transfer*. Hemisphere, Washington, DC

Tamonis, M. 1987. *Radiation and Combined Heat Transfer in Channels*. Springer-Verlag, New York

Thompson, J. F., Warsi, Z. U., Mastin, A. and Wayne, C. 1985. *Numerical Grid Generation, Foundation and Applications*. Elsevier, New York

Yang, G. and Ebadian, M. A. 1992. Combined radiation and convective heat transfer in simultaneously developing duct flow in a semi-circular and right triangular cross-section. *Wärme und Stoffübertragung*, **27** (3), 141–148

Yang, G. and Ebadian, M. A. 1991. Thermal radiation and laminar forced convection in the entrance region of a pipe with axial conduction and radiation. *Int. J. Heat Fluid Flow*, **12** (3), 202–209

Yang, G., Ebadian, M. A. and Campo, A. 1989. Combined radiation–convection in thermally developing gas flow in non-circular ducts. *Proc. 6th Int. Conf. Numer. Methods Laminar Turbulent Flow*, **6** (2), 1011–1021